

JGR Space Physics

RESEARCH ARTICLE

10.1029/2021JA029709

Key Points:

- We present a statistical study of the energy spectrum of electron microbursts observed by the FIREBIRD-II CubeSats
- Individual microbursts contain more electrons at a higher Auroral Electrojet as well as relatively more high-energy electrons
- The microburst scattering mechanism is more efficient at scattering low-energy electrons

Supporting Information:

Supporting Information may be found in the online version of this article.

Correspondence to:

A. T. Johnson,
arlotjohnson@gmail.com

Citation:

Johnson, A. T., Shumko, M., Sample, J., Griffith, B., Klumpar, D., Spence, H., & Blake, J. B. (2021). The energy spectra of electron microbursts between 200 keV and 1 MeV. *Journal of Geophysical Research: Space Physics*, 126, e2021JA029709. <https://doi.org/10.1029/2021JA029709>

Received 23 JUN 2021
Accepted 10 OCT 2021

© 2021. American Geophysical Union.
All Rights Reserved.

The Energy Spectra of Electron Microbursts Between 200 keV and 1 MeV

A. T. Johnson¹ , M. Shumko² , J. Sample¹ , B. Griffith³ , D. Klumpar¹, H. Spence⁴ , and J. B. Blake⁵ 

¹Physics Department, Montana State University, Bozeman, MT, USA, ²NASA's Goddard Space Flight Center, Greenbelt, MD, USA, ³Department of Earth and Space Sciences, University of Washington, Seattle, WA, USA, ⁴Physics Department, University of New Hampshire, Durham, NH, USA, ⁵Space Science Applications Laboratory, The Aerospace Corporation, El Segundo, CA, USA

Abstract This study investigates the energy spectrum of electron microbursts observed by the Focused Investigations of Relativistic Electron Burst Intensity, Range, and Dynamics II (FIREBIRD-II, henceforth FIREBIRD) CubeSats. FIREBIRD is a pair of CubeSats, launched in January 2015 into a low Earth orbit, which focuses on studying electron microbursts. High-resolution electron data from FIREBIRD-II consist of 5 differential energy channels between 200 keV and 1 MeV and a >1 MeV integral channel. This covers an energy range that has not been well studied from low Earth orbit with good energy and time resolution. This study aims to improve the understanding of the scattering mechanism behind electron microbursts by investigating their spectral properties and their relationship with the equatorial electron population under different geomagnetic conditions. Microbursts are identified in the region of the North Atlantic where FIREBIRD only observes electrons in the bounce loss cone. The electron flux and exponential energy spectrum of each microburst are calculated using a FIREBIRD instrument response modeled in GEANT4 (GEometry AND Tracking) and compared with the near-equatorial electron spectra measured by the Van Allen Probes. Microbursts occurring when the Auroral Electrojet (AE) index is enhanced tend to carry more electrons with relatively higher energies. The microburst scattering mechanism is more efficient at scattering electrons with lower energies; however, the difference in scattering efficiency between low and high energy is reduced during periods of enhanced AE.

1. Introduction

Microbursts are short intensifications of electron precipitation into the atmosphere lasting up to a few hundred milliseconds. The term microburst was first used by Anderson and Milton (1964) to describe enhancements in balloon observations of ≤ 100 keV bremsstrahlung X-rays caused by electrons impacting the atmosphere. Later, balloon observations up to 300 keV revealed microbursts to be a significant loss process in the dayside magnetosphere (Parks, 1978). More recently, relativistic (>1 MeV) electron microbursts have been observed in situ by the spacecraft (Blake et al., 1996; Imhof et al., 1992; Lorentzen, Blake, et al., 2001).

Microbursts are most likely generated through resonant interactions with whistler-mode chorus (Breneman et al., 2017; Nakamura et al., 2000). Previous studies have shown that microburst activity coincides with the time and location of whistler-mode chorus (Lam et al., 2010; Lorentzen, Blake, et al., 2001; Lorentzen, Looper, & Blake, 2001; Oliven & Gurnett, 1968) and that microbursts have a similar scale size to chorus wave packets (Agapitov et al., 2018; Shumko et al., 2020). In addition, theoretical studies have established the possible effectiveness of scattering by whistler-mode chorus (Chang & Inan, 1983; Chen et al., 2020; Miyoshi et al., 2015, 2020; Rosenberg et al., 1990).

The importance of microbursts to the overall magnetospheric system could be significant. Using storm time Solar, Anomalous, and Magnetospheric Particle EXplorer (SAMPEX) Heavy Ion Large Telescope (HILT) data, it has been estimated that microbursts are capable of emptying the outer radiation belt of 1 MeV electrons on the order of a day (Lorentzen, Looper, & Blake, 2001; O'Brien et al., 2004; Thorne et al., 2005). This represents a significant source of electron loss from the magnetosphere.

An important factor to understand microbursts and their relationship with the magnetospheric system is the energy spectrum. Comparing the energy spectrum of a microburst to the background energy spectrum in the radiation belts gives insight into the processes that scatter microburst electrons and helps determine the importance of microbursts as a loss process at various energies. Previous studies of the microburst energy spectrum have focused on lower energy microbursts from tens to a couple hundred keV (e.g., Anderson et al., 1966; Lampton, 1967; Lee et al., 2005, 2012; Reinard et al., 1997) or relativistic energies of >1 MeV (e.g., Imhof et al., 1992), but the energy range from a few hundred keV to 1 MeV has not been well studied. Blake et al. (1996) compared microburst detections on the 150 keV and >1 MeV channels of the HILT detector on SAMPEX and found they were not always correlated, which could indicate a difference in generation mechanism. Lorentzen, Blake, et al. (2001) showed that chorus propagating obliquely could explain why microbursts of different energies are not correlated, despite having the same driver. To determine if the generation mechanism for microbursts with tens of keV and MeV energies is different, it is important to study the intervening energies.

This study uses microburst data from low Earth orbit collected by the FIREBIRD CubeSat mission (Johnson et al., 2020; Spence et al., 2012) to investigate the energy spectrum of microbursts from 200 keV to 1 MeV. These spectra are compared with near-equatorial observations by the Magnetic Electron Ion Spectrometer (MagEIS) aboard the Van Allen Probes (Blake et al., 2013) to estimate the efficiency of the scattering mechanism at different energies and levels of geomagnetic activity.

2. Instrument Description

FIREBIRD-II (Johnson et al., 2020) is a pair of National Science Foundation CubeSats termed Flight Unit (FU) 3 and FU4. They were launched on January 31, 2015, into a 98° inclination and 400 × 600 km orbit. Each unit contains two silicon solid-state detectors referred to as the collimated and surface detectors. These detectors are identical except for an aluminum collimator over the collimated detector, which reduces the field of view and geometric factor of that detector. The surface detector on FU4 never functioned in orbit and the surface detector on FU3 began behaving anomalously around July 2015, so only the collimated data are used in this study. In the first few days of the mission, the spacecraft were very near each other in space and were able to simultaneously detect microbursts (Crew et al., 2016; Shumko et al., 2018). The spacecraft separated beyond the scale size of a microburst within just a few days, so for the purposes of this study, the spacecraft were treated independently.

FIREBIRD produces far more data than can be practically downloaded, so a campaign strategy is used. In each campaign, the spacecraft takes data until memory is filled, typically about 3–4 weeks; then, the instrument is turned off until a selected subset of data has been downloaded. Over the course of the mission, FIREBIRD has been taking data around a third of the time with the remaining two thirds mostly used for downloading data. FIREBIRD produces a 6-s cadence data product for two of the energy channels, which is used in combination with geomagnetic activity and satellite conjunctions to select times of high-resolution data to download. This results in a selection bias for the events chosen to be downloaded. It is difficult to be certain how this bias manifests but it is likely that weak or isolated microbursts will be underrepresented, since they have a minimal effect on the 6-s data. Campaigns have been configured with time cadences of 12.5, 18.75, and 50 ms, with 18.75 ms most common in the early mission and 50 ms most common in the later mission. In addition, starting with campaign 21, the energy channel boundaries were shifted to cover the low-energy range in finer resolution. This study uses data from campaigns 1–22, so campaigns with each cadence rate and energy boundary selection are used for spectral calculations.

MagEIS (Blake et al., 2013) is an instrument suite aboard each of NASA's Van Allen Probes measuring electrons and ions. The Van Allen Probes were launched in August 2012 on a near-geostationary transfer orbit, which samples the near-equatorial radiation belts from an altitude of about 600 km up to a geocentric distance near 6 R_E . Each probe spins with a period of about 11 s, allowing the sampling of different pitch angles. The MagEIS suite is composed of four instruments, which collectively cover electron energies from about 20 keV to 4.8 MeV. This study uses the electron flux values from MagEIS in the range from 200 to 1,200 keV to mimic the FIREBIRD energy range and in the pitch angle bin closest to the loss cone.

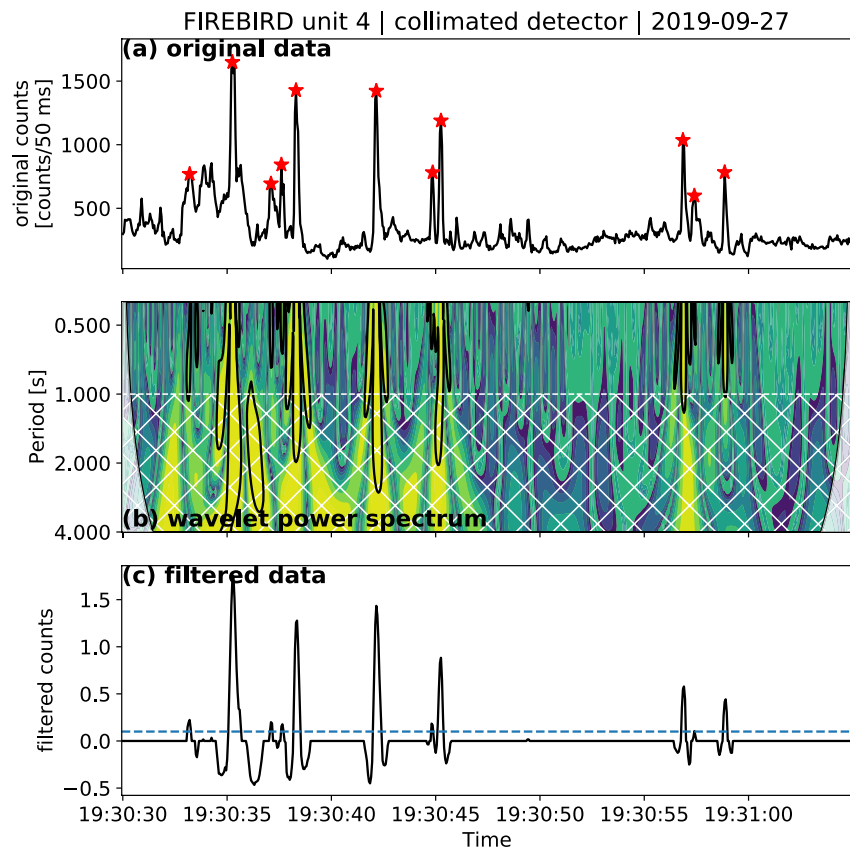


Figure 1. An example of the wavelet detection algorithm used to identify microbursts. (a) Original data from the 223.8 keV energy channel of FU4. Stars mark the peaks of identified microbursts. (b) The wavelet power spectrum of the data. Regions where the wavelet power spectrum exceeds the 95% confidence level of a red noise power spectrum are shown with bold contours. The white hatched region has Fourier periods longer than 1 s and are filtered out. (c) The filtered wavelet spectrum transformed back to the time domain. Times that exceed a threshold of 0.1, shown by the horizontal dashed line, are considered microbursts. Negative counts represent an anticorrelation with the wavelet.

3. Event Selection

FIREBIRD high-resolution data from campaigns 1–22 (February 2015–May 2019) were analyzed for this study. Candidate events were identified using a wavelet transformation and filtering similar to the analysis described in Torrence and Compo (1998). The wavelet used in the transform is the Second Derivative of Gaussian, which has a similar shape to a microburst. This wavelet is convolved with the data to create a power spectrum as a function of Fourier period and time. Microbursts with a similar width as the wavelet will strongly convolve and have a higher power. In order to detect a variety of possible microburst widths, this analysis was performed several times with wavelet widths ranging from twice the data cadence up to 1 s.

An example of this process is shown in Figure 1. Figure 1a shows high-resolution data from the 223.8 keV energy channel on FU4. Figure 1b shows the corresponding wavelet power spectrum. Times with possible microbursts are identified by filtering the wavelet spectrum to the times of significant power lasting no longer than 1 s. The power is considered significant when it rises above the 95% confidence level of a red noise power spectrum, marked with bold contours in Figure 1b. The white hatched area in Figure 1b covers periods longer than 1 s. Times that meet both of these criteria are inverse transformed back to the time domain, shown in Figure 1c, and will be considered a microburst candidate if the time series is peaked and above a 0.1 count threshold. A negative value in the filtered data corresponds to an anticorrelation between the original data and the wavelet. The peaks of identified microbursts are marked with stars in Figure 1a. This algorithm identified 11,866 and 10,789 microburst candidates on FU3 and FU4, respectively.

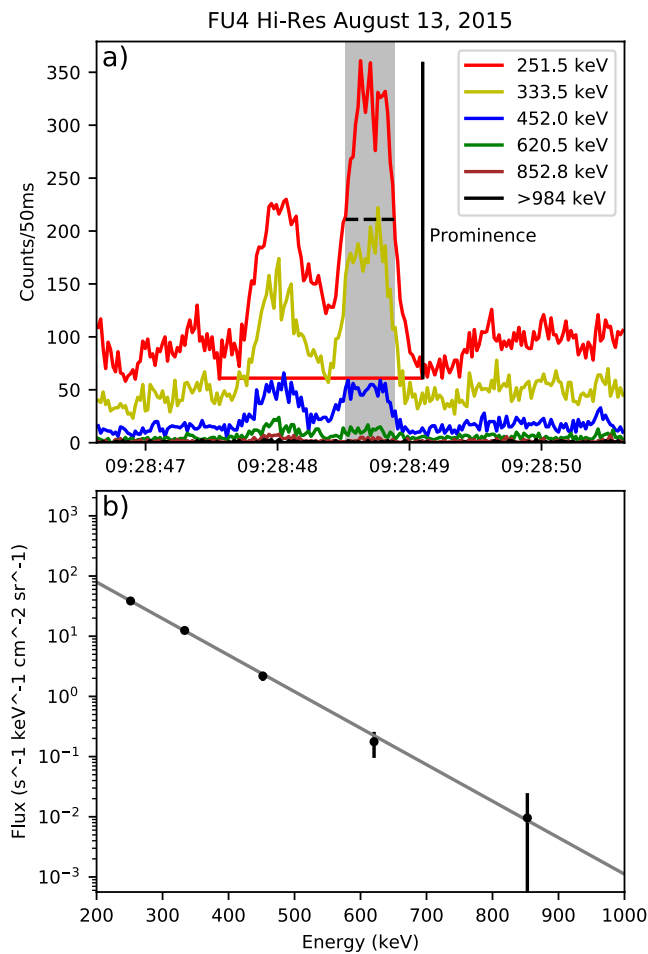


Figure 2. Example microburst and fit energy spectrum. Panel (a) shows the FIREBIRD time series data. The shaded gray area represents the time range each energy in the microburst was integrated over, calculated at half prominence in the lowest energy channel as shown with the dashed horizontal black line. The horizontal red line represents the background levels for the 251.5-keV channel. Panel (b) shows the GEANT-determined flux in each energy channel and best-fit e-folding function.

To reduce the effect of background precipitation and ensure that observations were of recently scattered microbursts, these events were further restricted to the region of the North Atlantic conjugate to the South Atlantic Anomaly, often referred to as the Bounce Loss Cone (BLC) region, similar to previous studies (e.g., Comess et al., 2013; Dietrich et al., 2010). Particles observed at FIREBIRD's altitude in this region have a conjugate mirror point in the southern hemisphere below 100 km. Electrons in the BLC will interact with the atmosphere and eventually be lost, with electrons mirroring deeper in the atmosphere being lost in fewer bounces. Around 3/4 of the identified microbursts had a mirror altitude below 50 km and would have been lost within a couple of bounce periods. The conjugate point of each candidate event was calculated using the Tsyganenko 1989 (T89) magnetic field model (Tsyganenko, 1989) keeping any event with a conjugate altitude below 100 km, a latitude between 0 and 80, and a longitude between -90 and 60 . These additional criteria are met by 1,612 and 1,256 candidate events on FU3 and FU4, respectively.

The remaining candidate events were then independently reviewed by two authors and any events both agreed were microbursts were selected for this study. This manual review is necessary due to the high number of false positives in the automatically detected candidates. Automatic detection in FIREBIRD data is challenging due to occasional data drop-outs where count rates go to near zero, saturation effects, and missing data points in the early mission. Other methods of detection have been tried, such as the method described in O'Brien et al. (2003), but also give a large number of false positives. The manual review was carried out by two authors independently to mitigate any bias that might be introduced. Of the 2,868 candidates identified, 786 were agreed to be microbursts, 1,763 were agreed to not be microbursts, and the remaining 319 had the authors' disagree. This leaves a final set of 400 microburst events on FU3 and 386 microburst events on FU4. Much of the following analysis utilizes the Auroral Electrojet (AE) index, which was available through February 2018. There were 277 events on FU3 and 227 events on FU4 with AE data available.

4. Analysis

Each identified microburst was fit with an assumed exponential function.

Figure 2 shows an example microburst observed by FU4 and the resulting fit. For each microburst, the prominence was calculated, defined as the vertical distance between the peak and its lowest contour line. The lowest contour in the 251.5-keV channel appears as the horizontal red line in Figure 2a. This is considered the background level and is subtracted from the count data. To mitigate fluctuations due to Poisson noise, the counts in each energy channel are integrated. The integration window is determined as the width of the peak in the lowest energy channel at half prominence, which is equivalent to the full width at half maximum after the background subtraction. The dashed horizontal black line in Figure 2a represents the height of half prominence and the shaded area shows the integration window.

The count rates were then converted to flux using the assumed exponential shape and the energy-dependent geometric factors determined by the GEANT4 (GEometry AND Tracking) (Agostinelli et al., 2003) FIREBIRD mass model described in Johnson et al. (2020). The geometric factors determined by the model account for effects such as an electron penetrating the detector and not depositing its full energy or scattering into the detector after a prior interaction with another part of the spacecraft. The flux was first estimated from the counts by dividing using an approximate geometric factor and the energy bin width. An exponential flux function of the form $J(E) = J_0 e^{-(E/E_0)}$ was then fit to these fluxes, where $J(E)$ is the flux at energy E , J_0 is a measure of intensity, and E_0 is the e-folding energy. The fitted function was then integrated with

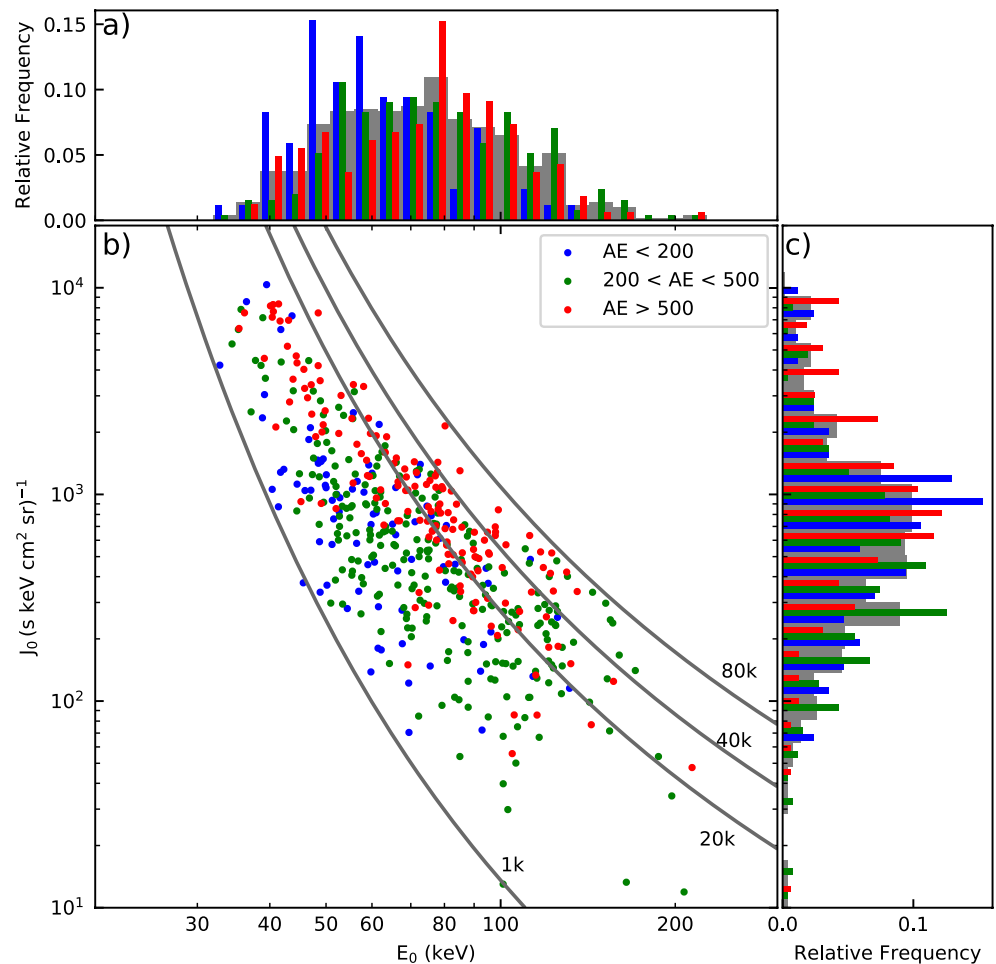


Figure 3. Comparison of E_0 and J_0 for each microburst with AE data in the study. Panel (a) shows a histogram of E_0 and panel (c) shows a histogram of J_0 . The histograms are normalized by the number of microbursts in each AE bin. Gray bars behind show the distribution for all microbursts. Panel (b) shows the value of E_0 and J_0 for each microburst. Solid lines in panel (b) show contours of constant total counts per second. Contours are at 1, 20, 40, and 80 thousand counts per second.

the GEANT-determined geometric factors to model the counts that FIREBIRD would observe. The parameters of the flux function were then iterated to find the best agreement between the observed and modeled count rates.

Figure 2b shows the GEANT-determined flux values in the 5 differential energy channels and the best-fit function. To calculate the flux in each energy channel, an effective geometric factor is first found by dividing the modeled count rates by the value of the flux function at the center of the energy channel. The observed count rates and their Poisson error are then divided by this effective geometric factor and shown as the black points and error bars in Figure 2b. The distribution of E_0 and J_0 is shown in Figure 3 for all microbursts with AE data and will be described in the next section.

For each microburst observed on FIREBIRD, a corresponding energy spectrum was found on each Van Allen Probe. Times of MagEIS data to analyze were selected as the nearest crossing of the microburst's L shell within 2 h in time, but at any MLT difference. In most cases, the background energy spectrum observed by MagEIS will not significantly vary by MLT due to the drift period of these energies being no more than a few tens of minutes. The distributions of the time and MLT difference are shown in Figures S1 and S2 in Supporting Information S1. The distribution of MLT differences consists of several peaks, which is explained by the campaign structure of the FIREBIRD mission. In between data campaigns, the orbital tracks of FIREBIRD and the Van Allen Probes precess relative to each other, leaving some MLT differences better sampled.

Pitch angle-resolved MagEIS data from 200 to 1,200 keV were used to investigate the energy spectrum of the source equatorial electrons. The pitch angle bin nearest to 0° (northward electrons) was used when available; otherwise, the pitch angle bin nearest to 180° was used instead. These bins predominantly represent the trapped population nearest to the loss cone, and therefore, the population is most likely to be scattered into a microburst. Occasionally, these bins will include the electrons already in the loss cone, but this is not a significant effect. At many times, the spin axis of the Van Allen Probes is oriented such that the loss cone is not sampled at all. At times, when the loss cone is sampled, it will be just a couple of degrees wide, which represents a small portion of the solid angle measured by the 16.4° wide pitch angle bin. The analysis was also performed with the omnidirectional MagEIS count data, which yielded similar results.

The MagEIS flux data were then fit with an assumed exponential flux function for comparison to FIREBIRD. The most common spectral shapes observed by MagEIS are exponential, power law, and bump-on-tail with exponential spectra, dominating in the outer radiation belt outside of the plasmopause (Zhao et al., 2019). The plasmopause location was calculated for each microburst event using the plasmopause model from O'Brien and Moldwin (2003) and the AE index. According to this model, all of the microburst events occurred outside the plasmopause, and most occurred at least 1 L from the plasmopause, so the assumption of an exponential spectral shape is not unreasonable. This is consistent with previous studies, which found most microbursts occur outside of the plasmopause (Douma et al., 2017; Johnston & Anderson, 2010). To filter any nonexponential spectral shapes, the standard deviation error is calculated for E_0 in each fit and must be less than 15% to be included.

5. Discussion

The distributions of the microbursts in the intensity J_0 and e-folding energy E_0 are shown in Figure 3. Each microburst is colored according to the value of the AE index at the time of the burst. Figures 3a and 3c are histograms for each parameter showing the relative occurrence rate for each AE value with the gray bars representing all microbursts. Each data set in the histogram has been normalized by the number of events in the bin. Of the 504 identified microbursts, 85 occurred during an AE < 200, 255 occurred during an AE between 200 and 500, and the remaining 164 occurred during an AE > 500. The solid lines in Figure 3b are contours representing the total number of electrons across all energies that would be observed by FIREBIRD. The total counts are determined by applying the FIREBIRD GEANT model to the exponential flux function for a given E_0 and J_0 pair and summing the response of all energy channels. Contours are drawn at 1, 20, 40, and 80 thousand counts per second.

The low J_0 boundary of the spectral distribution in Figure 3b appears to follow the 1,000 count per second contour line. It is likely that this boundary is an artifact representing the minimum counts needed for a microburst to be identified and successfully fit on FIREBIRD. As a comparison, Lee et al. (2005) used data from STSAT-1 to characterize the energy spectrum of microbursts between 170 and 330 keV with 30 energy channels. Lee et al. (2005) measured an E_0 of 19–20 keV in quiet conditions and 39–41 keV in storm times. An E_0 of 40 keV is at the low end of the distribution observed on FIREBIRD and no events with an E_0 below 30 keV were observed. For a microburst with a 20-keV e-folding energy to deposit enough counts to be observed on FIREBIRD, assumed here to be 1,000 counts per second, a J_0 around 10^6 would be required. It is possible that the lowered FIREBIRD energy channel boundaries beginning in campaign 21 would be sensitive to microbursts with a lower E_0 , but there were not enough events in campaigns 21 and 22 to get a statistically significant result.

The high J_0 boundary of the distribution in Figure 3b does not follow the count contour lines. At an E_0 of 50 keV, the bursts with the highest J_0 are near the 20,000 count/second contour, but at an E_0 of 150 keV almost 80,000 counts per second can be observed in the most intense bursts. This increase in electrons contained in a microburst could be explained by an increase in source electrons near the equator to be scattered or an improvement in the scattering efficiency of the microburst generation mechanism as AE increases or some combination of the two. If this boundary were due to instrumental effects, the opposite trend would be expected. Events observed by FIREBIRD are processed through a Wilkinson rundown Analog-Digital Converter with a dead time linearly proportional to the energy deposited into the detector by the event. Therefore, a 1-MeV electron will take 5 times longer to process than a 200-keV electron. This means fewer

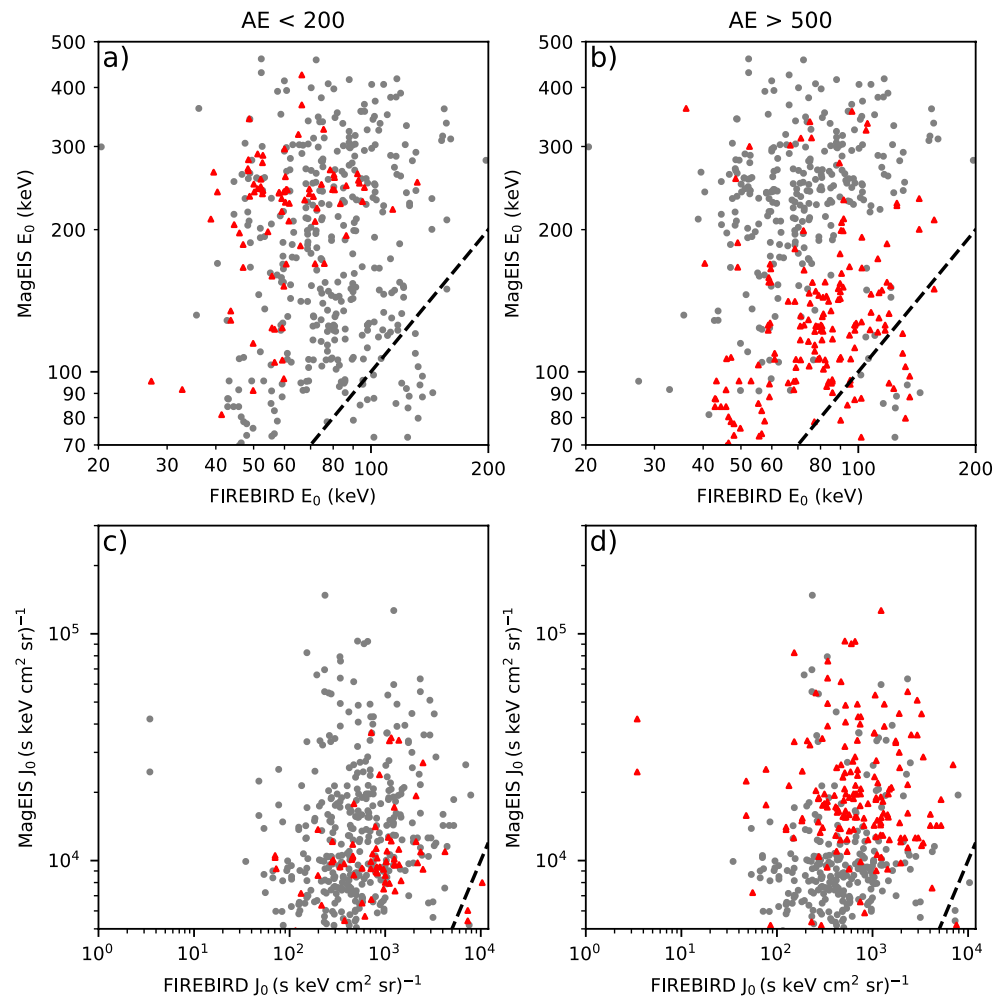


Figure 4. Comparison of E_0 and J_0 between FIREBIRD and MagEIS. Panels (a and b) show a comparison of E_0 and panels (c and d) show a comparison of J_0 . All microbursts are plotted in each panel, with microbursts satisfying the AE condition highlighted as red triangles. Panels (a and c) highlight Auroral Electrojet (AE) <200 and panels (b and d) highlight AE > 500. The dashed line in each panel indicates where the parameters are equal.

electrons are needed before the saturation effects will be observed during periods with relatively more high-energy electrons.

The distribution in Figure 3 varies with the AE index. Microbursts that occur during the times of high AE tend to have a higher E_0 than microbursts at a lower AE with a similar J_0 , and microbursts with a similar E_0 tend to have a higher J_0 at high AE. This is also reflected in Figure 3b by high AE microbursts carrying more electrons. The histograms in Figures 3a and 3c show this trend as well, although it is blurred due to looking at microbursts of all E_0 or J_0 instead of a specific value.

There is a substantial overlap between the AE bins, suggesting there may be other compounding effects that have not been accounted for. Variations based on L or MLT were investigated separately but no clear pattern was found. A possibility that cannot be investigated by FIREBIRD is a dependence on pitch angle. If the microburst scattering mechanism is able to scatter certain energies deeper into the loss cone, the energy spectrum would develop a dependence on pitch angle. FIREBIRD experiences a slow tumble, which causes it to sample a range of pitch angles. The precise nature of the tumble is unknown, and there is no pointing information to quantify it, so it is unclear what pitch angles are being sampled.

To further investigate the nature of the microburst scattering mechanism, the energy spectrum observed on FIREBIRD was compared with MageIS aboard the Van Allen Probes. Microburst electrons are rapidly scattered from the trapped population of electrons near the loss cone, so comparing their spectra can reveal the properties of the scattering mechanism. Figure 4 shows a comparison of both E_0 and J_0 and highlights how the relationship changes with AE. Figures 4a and 4b compare E_0 and Figures 4c and 4d compare J_0 . Each panel shows all microbursts in gray and highlights the microbursts meeting the AE condition as red triangles. Panels on the left (4a and 4c) highlight points observed at AE < 200, while panels on the right (4b and 4d) highlight points at AE > 500. The dashed line in each panel indicates where the parameters are equal.

Almost every observed microburst in Figures 4a and 4b appears above the dashed line indicating that a lower E_0 was observed on FIREBIRD than on MageIS. This suggests the microburst scattering mechanism is more efficient at scattering lower energy electrons. Furthermore, microbursts observed during times of higher AE in Figure 4b have a closer agreement in E_0 between the two missions. Considering a higher AE is also associated with more total electrons (Figure 3); this likely indicates that the scattering mechanism becomes more efficient at scattering high-energy electrons as AE increases.

Figures 4c and 4d show all points above the dashed line indicating more electron flux near the equator than in the microbursts. Comparing Figure 4c with Figure 4d shows that a higher AE is associated with an enhanced J_0 on both instruments, although the enhancement is more pronounced on MageIS. The larger enhancement in the trapped population compared to the precipitating population indicates that as the trapped flux increases, the microburst scattering efficiency decreases, although the net effect is still an enhancement in the precipitating population.

6. Conclusion

We have presented a statistical study of the energy spectrum of microburst electrons between 200 keV and 1 MeV. Microbursts were identified on the FIREBIRD-II CubeSats and fit with an exponential energy spectrum. Using MageIS data on the Van Allen Probes, the microburst spectrum was compared with the spectrum of the source population near the equator. The microburst fit parameters and their relationship with the equatorial population were tested against MLT, L shell, and AE index.

We found no correlation between either E_0 or J_0 and MLT or L shell, but an increase in AE index is associated with an increase in both parameters. This increase is also reflected as an increase in the number of electrons in an individual microburst. A comparison of the microburst and source e-folding energies found that microbursts typically have a smaller E_0 , but an enhanced AE brought the e-folding energies into closer agreement. The values of J_0 for microbursts and the source population were also compared and it was found that an enhanced AE causes an increase in both the microburst J_0 and the source population J_0 .

Data Availability Statement

FIREBIRD-II data are publicly available at http://solar.physics.montana.edu/FIREBIRD_II/. All RBSP-ECT data are publicly available at the website <http://www.RBSP-ect.lanl.gov/>. The AE index used in this paper was provided by the WDC for Geomagnetism, Kyoto (<http://wdc.kugi.kyoto-u.ac.jp/wdc/Sec3.html>). The wavelet code for identifying microbursts was adapted from code written by Evgeniya Predybaylo, available at https://github.com/chris-torrence/wavelets/tree/master/wave_python.

References

- Agapitov, O., Mourenas, D., Artemyev, A., Mozer, F. S., Bonnell, J. W., Angelopoulos, V., et al. (2018). Spatial extent and temporal correlation of chorus and hiss: Statistical results from multipoint THEMIS observations. *Journal of Geophysical Research: Space Physics*, 123(10), 8317–8330. <https://doi.org/10.1029/2018JA025725>
- Agostinelli, S., Allison, J., Amako, K., Apostolakis, J., Araujo, H., Arce, P., et al. (2003). GEANT4-A simulation toolkit. *Nuclear Instruments and Methods in Physics Research, Section A: Accelerators, Spectrometers, Detectors and Associated Equipment*, 506(3), 250–303. [https://doi.org/10.1016/S0168-9002\(03\)01368-8](https://doi.org/10.1016/S0168-9002(03)01368-8)
- Anderson, K. A., Chase, L. M., Hudson, H. S., Lampton, M., Milton, D. W., & Parks, G. K. (1966). Balloon and rocket observations of auroral-zone microbursts. *Journal of Geophysical Research*, 71(19), 4617–4629. <https://doi.org/10.1029/jz071i019p04617>

Acknowledgments

FIREBIRD-II is supported by the National Science Foundation under Grant Nos. 0838034, 1339414, and 1035642. Processing and analysis of the MageIS data were supported by Energetic Particle, Composition, and Thermal Plasma (RBSP-ECT) investigation funded under NASA's Prime contract no. NASS-01072. A.T. Johnson was supported under NASA grant Nos. 80NSSC19K0265 and 80NSSC19K0842. M. Shumko acknowledges the support provided by the NASA Postdoctoral Program at the NASA's Goddard Space Flight Center, administered by Universities Space Research Association under contract with NASA.

- Anderson, K. A., & Milton, D. W. (1964). Balloon observations of X Rays in the Auroral Zone 3. *Journal of Geophysical Research*, 69(21). <https://doi.org/10.1029/jz069i021p04457>
- Blake, J., Looper, M., Baker, D., Nakamura, R., Klecker, B., & Hovestadt, D. (1996). New high temporal and spatial resolution measurements by SAMPEX of the precipitation of relativistic electrons. *Advances in Space Research*, 18(8), 171–186. [https://doi.org/10.1016/0273-1177\(95\)00969-8](https://doi.org/10.1016/0273-1177(95)00969-8)
- Blake, J. B., Carranza, P. A., Claudepierre, S. G., Clemmons, J. H., Crain, W. R., Dotan, Y., et al. (2013). *The Magnetic Electron Ion Spectrometer (MagEIS) Instruments Aboard the Radiation Belt Storm Probes (RBSP) Spacecraft* (Vol. 9781489974, pp. 383–421). The Van Allen Probes mission. https://doi.org/10.1007/978-1-4899-7433-4_12
- Breneman, A. W., Crew, A., Sample, J., Klumpar, D., Johnson, A., Agapitov, O., et al. (2017). Observations directly linking relativistic electron microbursts to Whistler Mode Chorus: Van Allen Probes and FIREBIRD II. *Geophysical Research Letters*, 44(22), 11265–11272. <https://doi.org/10.1002/2017GL075001>
- Chang, H. C., & Inan, U. S. (1983). Quasi-relativistic electron precipitation due to interactions with coherent VLF waves in the magnetosphere. *Journal of Geophysical Research*, 88(A1), 318–328. <https://doi.org/10.1029/ja088ia01p00318>
- Chen, L., Breneman, A. W., Xia, Z., & Zhang, X.-j. (2020). Modeling of bouncing electron microbursts induced by ducted chorus waves. *Geophysical Research Letters*, 47, 1–26. <https://doi.org/10.1029/2020GL089400>
- Comess, M. D., Smith, D. M., Selesnick, R. S., Millan, R. M., & Sample, J. G. (2013). Duskside relativistic electron precipitation as measured by SAMPEX: A statistical survey. *Journal of Geophysical Research: Space Physics*, 118(8), 5050–5058. <https://doi.org/10.1002/jgra.50481>
- Crew, A. B., Spence, H. E., Blake, J. B., Klumpar, D. M., Larsen, B. A., O'Brien, T. P., et al. (2016). First multipoint in situ observations of electron microbursts: Initial results from the NSF FIREBIRD II mission. *Journal of Geophysical Research: Space Physics*, 121(6), 5272–5283. <https://doi.org/10.1002/2016JA022485>
- Dietrich, S., Rodger, C. J., Clilverd, M. A., Bortnik, J., & Raita, T. (2010). Relativistic microburst storm characteristics: Combined satellite and ground-based observations. *Journal of Geophysical Research*, 115(A12), A12240. <https://doi.org/10.1029/2010JG015070>
- Douma, E., Rodger, C. J., Blum, L. W., & Clilverd, M. A. (2017). Occurrence characteristics of relativistic electron microbursts from SAMPEX observations. *Journal of Geophysical Research: Space Physics*, 112(A4), A00F08. <https://doi.org/10.1002/2017JA024067>
- Imhof, W. L., Voss, H. D., Mobilia, J., Datlowe, D. W., Gaines, E. E., McGlennon, J. P., & Inan, U. S. (1992). Relativistic electron microbursts. *Journal of Geophysical Research*, 97(A9), 13829. <https://doi.org/10.1029/92JA01138>
- Johnson, A. T., Shumko, M., Griffith, B., Klumpar, D. M., Sample, J., Springer, L., et al. (2020). The FIREBIRD-II CubeSat mission: Focused investigations of relativistic electron burst intensity, range, and dynamics. *Review of Scientific Instruments*, 91(3), 034503. <https://doi.org/10.1063/1.5137905>
- Johnston, W. R., & Anderson, P. C. (2010). Storm time occurrence of relativistic electron Microbursts in relation to the plasmapause. *Journal of Geophysical Research: Space Physics*, 115(2), A02205. <https://doi.org/10.1029/2009JA014328>
- Lam, M. M., Horne, R. B., Meredith, N. P., Glauert, S. A., Moffat-Griffin, T., & Green, J. C. (2010). Origin of energetic electron precipitation >30 keV into the atmosphere. *Journal of Geophysical Research: Space Physics*, 115(A4), A00F08. <https://doi.org/10.1029/2009JA014619>
- Lampton, M. (1967). Daytime observations of energetic auroral-zone electrons. *Journal of Geophysical Research*, 72(23), 5817–5823. <https://doi.org/10.1029/jz072i023p05817>
- Lee, J. J., Parks, G. K., Lee, E., Tsurutani, B. T., Hwang, J., Cho, K. S., et al. (2012). Anisotropic pitch angle distribution of 100 keV microburst electrons in the loss cone: Measurements from STSAT-1. *Annales Geophysicae*, 30(11), 1567–1573. <https://doi.org/10.5194/angeo-30-1567-2012>
- Lee, J. J., Parks, G. K., Min, K. W., Kim, H. J., Park, J., Hwang, J., & Park, H. Y. (2005). Energy spectra of ~170–360 keV electron microbursts measured by the Korean STSAT-1. *Geophysical Research Letters*, 32(13), 1–4. <https://doi.org/10.1029/2005GL022996>
- Lorentzen, K. R., Blake, J. B., Inan, U. S., & Bortnik, J. (2001). Observations of relativistic electron microbursts in association with VLF chorus. *Journal of Geophysical Research*, 106(A), 6017–6027. <https://doi.org/10.1029/2000JA003018>
- Lorentzen, K. R., Looper, M. D., & Blake, J. B. (2001). Relativistic electron microbursts during the GEM storms. *Geophysical Research Letters*, 28(13), 2573–2576. <https://doi.org/10.1029/2001GL012926>
- Miyoshi, Y., Oyama, S., Saito, S., Kurita, S., Fujiwara, H., Kataoka, R., et al. (2015). Energetic electron precipitation associated with pulsating aurora: EISCAT and Van Allen Probe observations. *Journal of Geophysical Research: Space Physics*, 120(4), 2754–2766. <https://doi.org/10.1002/2014JA020690>
- Miyoshi, Y., Saito, S., Kurita, S., Asamura, K., Hosokawa, K., Sakanoi, T., et al. (2020). Relativistic electron microbursts as high-energy tail of pulsating aurora electrons. *Geophysical Research Letters*, 47, e2020GL090360. <https://doi.org/10.1029/2020GL090360>
- Nakamura, R., Isowa, M., Kamide, Y., Baker, D. N., Blake, J. B., & Looper, M. (2000). SAMPEX observations of precipitation bursts in the outer radiation belt. *Journal of Geophysical Research: Space Physics*, 105(A7), 15875–15885. <https://doi.org/10.1029/2000ja900018>
- O'Brien, T. P., Looper, M. D., & Blake, J. B. (2004). Quantification of relativistic electron microburst losses during the GEM storms. *Geophysical Research Letters*, 31(4), L04802. <https://doi.org/10.1029/2003GL018621>
- O'Brien, T. P., Lorentzen, K. R., Mann, I. R., Meredith, N. P., Blake, J. B., Fennell, J. F., & Anderson, R. R. (2003). Energization of relativistic electrons in the presence of ULF power and MeV microbursts: Evidence for dual ULF and VLF acceleration. *Journal of Geophysical Research: Space Physics*, 108(A8), 1329. <https://doi.org/10.1029/2002JA009784>
- O'Brien, T. P., & Moldwin, M. B. (2003). Empirical plasmapause models from magnetic indices. *Geophysical Research Letters*, 30(4), 1152. <https://doi.org/10.1029/2002GL016007>
- Oliven, M. N., & Gurnett, D. A. (1968). Microburst phenomena: 3. An association between microbursts and VLF chorus. *Journal of Geophysical Research*, 73(7), 2355–2362. <https://doi.org/10.1029/ja073i007p02355>
- Parks, G. K. (1978). Microburst precipitation phenomena. *Journal of Geomagnetism and Geoelectricity*, 30, 327–341. <https://doi.org/10.5636/jgg.30.327>
- Reinard, A. A., Skoug, R. M., Datta, S., & Parks, G. K. (1997). Energy spectral characteristics of auroral electron microburst precipitation. *Geophysical Research Letters*, 24(5), 611–614. <https://doi.org/10.1029/97GL00377>
- Rosenberg, T. J., Wei, R., Detrick, D. L., & Inan, U. S. (1990). Observations and modeling of wave-induced microburst electron precipitation. *Journal of Geophysical Research*, 95, 6467–6475. <https://doi.org/10.1029/ja095ia05p06467>
- Shumko, M., Johnson, A. T., Sample, J. G., Griffith, B. A., Turner, D. L., O'Brien, T. P., et al. (2020). Electron microburst size distribution derived with AeroCube-6. *Journal of Geophysical Research: Space Physics*, 125(3), e2019JA027651. <https://doi.org/10.1029/2019JA027651>
- Shumko, M., Sample, J., Johnson, A., Blake, J. B., Crew, A., Spence, H., & Handley, M. (2018). Microburst scale size derived from multiple bounces of a microburst simultaneously observed with the FIREBIRD-II cubeSats. *Geophysical Research Letters*, 45, 8811–8818. <https://doi.org/10.1029/2018gl078925>

- Spence, H. E., Blake, J. B., Crew, A. B., Driscoll, S., Klumpar, D. M., Larsen, B. A., et al. (2012). Focusing on size and energy dependence of electron microbursts from the Van Allen radiation belts. *Space Weather*, 10(11), 10–12. <https://doi.org/10.1029/2012SW000869>
- Thorne, R. M., O'Brien, T. P., Shprits, Y. Y., Summers, D., & Horne, R. B. (2005). Timescale for MeV electron microburst loss during geomagnetic storms. *Journal of Geophysical Research: Space Physics*, 110(A9), A09202. <https://doi.org/10.1029/2004JA010882>
- Torrence, C., & Compo, G. P. (1998). A practical guide to wavelet analysis. *Bulletin of the American Meteorological Society*, 79(1), 61–78. [https://doi.org/10.1175/1520-0477\(1998\)079<0061:APGTWA>2.0.CO;2](https://doi.org/10.1175/1520-0477(1998)079<0061:APGTWA>2.0.CO;2)
- Tsyganenko, N. A. (1989). A magnetospheric magnetic field model with a warped tail current sheet. *Planetary and Space Science*, 37(1), 5–20. [https://doi.org/10.1016/0032-0633\(89\)90066-4](https://doi.org/10.1016/0032-0633(89)90066-4)
- Zhao, H., Johnston, W. R., Baker, D. N., Li, X., Ni, B., Jaynes, A. N., et al. (2019). Characterization and evolution of radiation belt electron energy spectra based on the Van Allen probes measurements. *Journal of Geophysical Research: Space Physics*, 124(6), 4217–4232. <https://doi.org/10.1029/2019JA026697>